

3D Forward and Back-Projection for X-Ray CT Using Separable Footprints with Trapezoid Functions

Yong Long and Jeffrey A. Fessler

Abstract—The greatest impediment to practical adoption of iterative methods for X-ray CT is the computation burden of cone-beam forward and back-projectors. Moreover, forward and back-projector accuracy is also crucial to iterative reconstruction methods. We previously described a computationally efficient projector that approximates the voxel footprint functions by the 2D separable products of trapezoid functions in the transaxial plane and rectangular functions in the axial direction [1], [2]. The separability of these footprint functions simplifies calculating their integrals over rectangular detector cells. We showed that this separable footprint (SF-TR) method was more accurate than the distance-driven (DD) method but with comparable computation time. This paper describes a new extension of that projector, called the SF-TT projector, that uses trapezoid functions in both directions. We show that using a trapezoid along the axial direction improves projector accuracy for voxels associated with larger cone angles. However, this improved accuracy requires increased computation compared to the rectangular approximation. Having both options available facilitates evaluation of the trade offs between accuracy and computation for different cone-beam geometries.

Index Terms—Cone-beam tomography, iterative tomographic image reconstruction, forward and back-projection, separable footprint

I. INTRODUCTION

Iterative statistical methods for 3D tomographic image reconstruction offer the potential for improved image quality and reduced X-ray dose, compared to conventional filtered back-projection (FBP) methods. The primary computational bottleneck in iterative reconstruction methods is forward and back-projection operations. The forward projection is roughly a discretized evaluation of the Radon transform, and the back-projector is its adjoint. Mathematically, an accurate forward projector must compute the convolution of the footprint of an image basis function with some detector blur model, such as a 2D rectangular function that represents the finite size of detector cells.

Numerous 3D forward and back-projection methods have been proposed [1]–[8]. Each method compromises between computational complexity and accuracy. Spherically symmetric basis functions (blobs) [5], [6] have radially symmetric footprints that conveniently are independent of the viewing angle, except for a magnification factor. However, when high accuracy is desired, blob footprints intersect many more detector cells than voxel footprints, increasing computation.

This work was supported in part by NIH grant P01-CA59827.

Y. Long and J. Fessler are with Dept. of Electrical Engineering and Computer Science, University of Michigan, Ann Arbor, MI 48109.

The distance-driven (DD) method [4] maps the horizontal and vertical boundaries of the image voxels and detector cells onto a common plane such as xz or yz plane, approximating their shapes by rectangles. It calculates the lengths of overlap along the transaxial direction and along the axial direction, and then multiplies them to get the area of overlap. The DD method has the largest errors when the X-ray source’s azimuthal angle is near odd multiples of $\pi/4$, where the transaxial footprint is approximately triangular rather than rectangular.

We proposed previously a separable footprint (SF-TR) projector [1] that approximates the voxel footprint functions as 2D separable functions with trapezoid and rectangle functions in the transaxial and axial directions respectively. The separability of these footprint functions greatly simplifies the calculation of their integrals over detector cells leading to an efficient implementation. The SF-TR method has similar computation speed as the DD projector, but is more accurate, reducing particularly the errors around odd multiples of $\pi/4$. The rectangle approximation in the axial direction is reasonable for smaller CT cone angles such as multi-slice detector geometries. However, for CT systems with larger cone angles ($> 10^\circ$), such as flat-panel detector geometries, the rectangle approximation becomes less accurate.

This paper describes a new separable footprint method for forward and back-projection called the SF-TT method. It approximates the voxel footprint functions using 2D separable functions with trapezoid functions in *both* the transaxial and axial directions. We show that the SF-TT projector is more accurate than the SF-TR projector, but requires more computation. To balance computation and accuracy, one may use the SF-TR projector for voxels associated with small cone angles (*i.e.*, near the plane of the X-ray source) where the rectangle approximation is adequate, and use the new SF-TT projector for voxels associated with larger cone angles.

The organization of this paper is as follows. Section 2 describes the cone-beam 3D system model, and introduces the SF-TT projector. Section 3 gives simulation results, including accuracy and speed comparison between the SF-TT and SF-TR projector as stand alone modules and within iterative image reconstruction. Finally, conclusions are in Section 5.

II. METHOD

A. Cone-Beam 3D System Model

For iterative image reconstruction, we forward project a discretized approximation of the continuous-space object $f(\vec{x})$

represented by a common basis function $\beta_0(\vec{x})$ superimposed on a $N_1 \times N_2 \times N_3$ Cartesian grid as follows:

$$f(\vec{x}) = \sum_{\vec{n}} f[\vec{n}] \beta_0\left((\vec{x} - \vec{c}[\vec{n}]) \oslash \vec{\Delta}\right), \quad (1)$$

where the sum is over the $N_1 \times N_2 \times N_3$ lattice that is estimated and $\vec{c}[\vec{n}] = (c_1[\vec{n}], c_2[\vec{n}], c_3[\vec{n}])$ denotes the center of the \vec{n} th basis function and $\vec{n} = (n_1, n_2, n_3) \in \mathbb{Z}^3$. The grid spacing is $\vec{\Delta} = (\Delta_1, \Delta_2, \Delta_3)$, and \oslash denotes element-wise division. We consider the case $\Delta_1 = \pm\Delta_2$ hereafter, but we allow $\Delta_1 \neq \Delta_3$, because voxels are often not cubic.

Axial cone-beam projection space is characterized by three independent indices (s, t, β) and two distance parameters (D_{sd}, D_{s0}) , where β denotes the angle of the source point counter-clockwise from the y axis, (s, t) denote the local coordinates on the 2D detector plane where the s -axis is perpendicular to the z -axis and the t -axis is parallel to the z -axis D_{sd} denotes the source to detector distance and D_{s0} denotes the source to rotation center distance.

The cone-beam projections of $f(\vec{x})$ are given by

$$p(s, t; \beta) = \int_{\mathcal{L}(s, t, \beta)} f(x, y, z) dl, \quad (2)$$

where

$$\mathcal{L}(s, t, \beta) = \left\{ \vec{p}_0 + \alpha \vec{e}_3 : \alpha \in \left[0, \sqrt{D_{sd}^2 + s^2 + t^2}\right] \right\},$$

and \vec{e}_3 denotes the direction vector of a ray from the source position \vec{p}_0 to a point \vec{p}_1 on the detector plane.

Assume that the detector blur $h(s, t)$ is shift invariant, independent of β , and acts only along the s and t coordinates. Then the mean projections satisfy

$$\bar{y}_\beta[s_k, t_l] = \iint h(s_k - s, t_l - t) p(s, t; \beta) ds dt, \quad (3)$$

where (s_k, t_l) denotes the center of detector cell specified by indices (k, l) for $k = 0, \dots, N_s - 1$ and $l = 0, \dots, N_t - 1$.

Substituting the basis expansion model (1) for the object into (3) and using (2) leads to the linear model

$$\bar{y}_\beta[s_k, t_l] = \sum_{\vec{n}} a_\beta[s_k, t_l; \vec{n}] f[\vec{n}], \quad (4)$$

where the elements of cone-beam system matrix \mathbf{A} are samples of the following cone-beam projection of a single basis function centered at $\vec{c}[\vec{n}]$:

$$a_\beta[s_k, t_l; \vec{n}] = F(s_k, t_l; \beta; \vec{n}), \quad (5)$$

where the ‘‘blurred footprint’’ function is

$$F(s, t; \beta; \vec{n}) \triangleq \iint h(s - s', t - t') q(s', t'; \beta; \vec{n}) ds' dt',$$

and $q(s, t; \beta; \vec{n})$ denotes the cone-beam footprint of basis function $\beta_0\left((\vec{x} - \vec{c}[\vec{n}]) \oslash \vec{\Delta}\right)$, *i.e.*,

$$q(s, t; \beta; \vec{n}) = \int_{\mathcal{L}(s, t, \beta)} \beta_0\left((\vec{x} - \vec{c}[\vec{n}]) \oslash \vec{\Delta}\right) dl. \quad (6)$$

The goal of forward projectors is to compute (4) rapidly but accurately.

A simple model for the detector blur is

$$h(s, t) = \frac{1}{r_s r_t} \text{rect}\left(\frac{s}{r_s}\right) \text{rect}\left(\frac{t}{r_t}\right), \quad (7)$$

where r_s and r_t denote the width along s and t respectively. This model accounts for the finite size of the detector elements.

B. Separable Footprint Projector with Trapezoid Functions (SF-TT)

The footprints of voxel basis functions can be computed analytically for cone-beam geometries [9, p. 104]. Fig. 1 shows an example of a true footprint and its profiles. This 2D function is approximately separable except for small areas at the upper left and lower right corner.

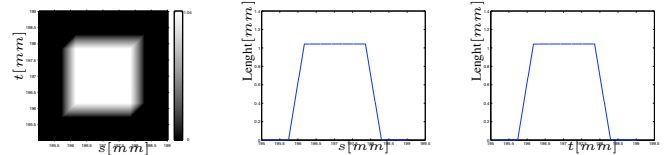


Fig. 1. The exact footprint function $q(s, t; \beta; \vec{n})$ and its profiles of a voxel with $\Delta_1 = \Delta_2 = \Delta_3 = 1\text{mm}$ centered at $(93, 93, 93)\text{mm}$ under a flat-detector cone-beam geometry with $D_{sd} = 949\text{mm}$ and $D_{s0} = 541\text{mm}$ when $\beta = 0^\circ$. The azimuthal and polar angle of the ray connecting the source and the voxel center are 11.7° and 11.5° respectively.

Inspired by the shape of the true footprint, we approximate voxel footprints as 2D separable functions with trapezoid functions in *both* the transaxial and axial direction as follows,

$$q(s, t; \beta; \vec{n}) \approx \Delta_x l(\beta; \vec{n}) \text{trap}(s; \tau_0, \tau_1, \tau_2, \tau_3) \cdot \text{trap}(t; \xi_0, \xi_1, \xi_2, \xi_3), \quad (8)$$

where

$$l(\beta; \vec{n}) \triangleq \frac{1}{|\cos(\theta_0)| \cdot \max\{|\cos(\varphi_0)|, |\sin(\varphi_0)|\}},$$

$$\text{trap}(a; b_0, b_1, b_2, b_3) \triangleq \begin{cases} \frac{a-b_0}{b_1-b_0}, & b_0 < a < b_1 \\ 1, & b_1 \leq a \leq b_2 \\ \frac{b_3-a}{b_3-b_2}, & b_2 < a < b_3 \\ 0, & \text{otherwise,} \end{cases} \quad (9)$$

where θ_0 and φ_0 denote the polar and azimuthal angles of the ray connecting the source and center of the \vec{n} th voxel respectively, τ_0, τ_1, τ_2 and τ_3 denote vertices of the trapezoid function which are at the exact locations as those of the true footprint function in the s direction, and ξ_0, ξ_1, ξ_2 and ξ_3 denote vertices of the trapezoid function in the t direction which are the projected t coordinates of four axial boundaries of the voxel.

Using the projections of boundaries of the voxel basis function as the boundaries of the approximate separable footprints ensures the depth-dependent magnification of the cone-beam geometry is modeled accurately. It also allows the approximated separable footprints to adapt their shapes according to relative positions of the source, detector and voxels, as true footprints do. For example, for a voxel centered at the origin, its axial footprint is approximately a rectangular function as

shown in [1, Fig. 1], instead of a trapezoid function. For this voxel $\text{trap}(t; \xi_0, \xi_1, \xi_2, \xi_3)$ is almost a rectangle because $\xi_0 \approx \xi_1$ and $\xi_2 \approx \xi_3$ because ξ_0, ξ_1, ξ_2 and ξ_3 are the projected t coordinates of four axial boundaries of the voxel.

To accelerate the computation of the SF-TT projector, we adopt the acceleration method used by the SF-TR projector [1]. We initially ignore $l(\beta; \vec{n})$ by setting $l(\beta; \vec{n}) = 1$ for all the voxels at any projection view, and then scale the “blurred footprint” functions by multiplying them by a ray-dependent scale factor.

III. RESULT

A. Forward and Back-Projector as Single Modules

We simulated an axial cone-beam flat-detector X-ray CT system with a detector size of $N_s \times N_t = 512 \times 512$ cells spaced by $\Delta_s = \Delta_T = 1\text{mm}$ with $N_\beta = 984$ angles over 360° . The source to detector distance D_{sd} is 949mm, and the source to rotation center distance D_{s0} is 541mm. We included a rectangular detector response (7) with $r_s = \Delta_s$ and $r_t = \Delta_T$.

We implemented the SF-TR and SF-TT projector in ANSI C using single precision. The DD projector was provided by De Man *et al.*, also implemented in ANSI C.

1) *Maximum Errors of Forward Projectors:* We define the maximum error as

$$e(\beta; \vec{n}) = \max_{s,t \in \mathbb{R}} |F(s, t; \beta; \vec{n}) - F_{ap}(s, t; \beta; \vec{n})|, \quad (10)$$

where $F_{ap}(s, t; \beta; \vec{n})$ is any of the approximate blurred footprints by the SF-TR, SF-TT and DD methods. We generated the true footprint $F(s, t; \beta; \vec{n})$ in (5) by linearly averaging 1000×1000 analytical line integrals of rays sampled over each detector cell.

We compared the maximum errors of the forward SF-TR, SF-TT and DD projectors for a voxel with $\Delta_x = \Delta_y = \Delta_z = 1\text{mm}$ centered at $(0, 0, -100)\text{mm}$. Since the voxel is centered at the origins of x and y axes, we choose $N_\beta = 180$ angles over only 90° rotation. Fig. 2 shows the results on a logarithmic scale. The maximum errors of the SF-TT projector are smaller than those of the SF-TR and DD projector, *e.g.*, the maximum errors of the DD and SF-TR projector are about 18 and 3 times larger than that of the SF-TT projector when $\beta = 45^\circ$. We also compared the maximum errors for a voxel centered at $(100, 150, -100)\text{mm}$. We choose $N_\beta = 720$ angles over 360° rotation due to the offsets of this voxel in the x and y direction. Fig. 3 shows the results. The maximum errors over 360° rotation of the DD and SF-TR projector are about 13 and 3 times of that of the SF-TT projector.

2) *Speed of Forward and Back-projectors:* We compared the computation times of the SF-TR, SF-TT and DD projectors using an image whose size is $N_1 = 512, N_2 = 512, N_3 = 128$ and spacing is $\Delta_1 = \Delta_2 = \Delta_3 = 0.5\text{mm}$. We evaluated the elapsed time using the average of 5 projector runs on a 8-core Sun Fire X2270 server with 2.66 GHz Xeon X5500 processors. Because of the “hyperthreading” of these Nehalem cores, we used 16 POSIX threads to parallelize the projection operation across views. (We found that using 16 threads reduced computation time by only about 10% compared to using 8 threads.)

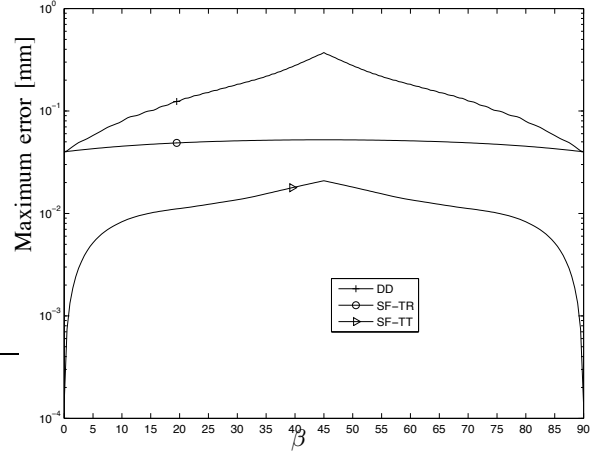


Fig. 2. Maximum error comparison between the forward DD, SF-TR and SF-TT projector for a voxel centered at $(0, 0, -100)\text{mm}$.

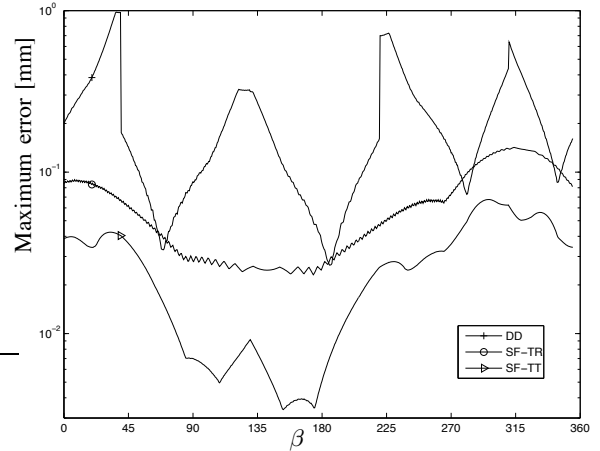


Fig. 3. Maximum error comparison between the forward DD, SF-TR and SF-TT projector for a voxel centered at $(100, 150, -100)\text{mm}$.

Table I summarizes computation times. The computation times of the SF-TR and DD projector are about the same, whereas the SF-TT projector is about 2 times slower. Of course execution times depend on code implementation.

B. Forward and Back-projectors within Iterative Reconstruction

We also compare the SF-TT projector and the SF-TR projector within an iterative reconstruction method. (We already showed the SF-TR method provides less artifacts in the reconstructed images than the DD method in [1]).

We simulated a X-ray axial cone-beam CT system with a flat-panel detector of 512 detector channels for 512 slices

Projectors	SF-TT	SF-TR	DD
Forward time (seconds)	91	35	46
Backward time (seconds)	92	44	49

TABLE I
SPEED COMPARISON OF THE SF-TT, SF-TR AND DD FORWARD AND BACK PROJECTORS.

($N_s = 512, N_t = 512$) by $N_\beta = 984$ views over 360° . The size of each detector cell is $\Delta_s \times \Delta_T = 1 \times 1 \text{ mm}^2$. The source to detector distance is $D_{sd} = 949.075 \text{ mm}$, and the source to rotation center distance is $D_{s0} = 541 \text{ mm}$. A quarter detector offset in the s direction is included to reduce aliasing.

We modified the 3D Shepp-Logan digital phantom to include several ellipsoids centered at the $z = 112.5$ plane because the trapezoid approximation of the SF-TT method is more realistic than the rectangle approximation of the SF-TR method especially for voxels far away from the origin. The field of view (FOV) is $250 \times 250 \times 250 \text{ mm}^3$, implying $256 \times 256 \times 256$ voxels with a resolution of $0.9766 \times 0.9766 \times 0.9766 \text{ mm}^3$. We simulated noiseless cone-beam projection measurements from the Shepp-Logan phantom by linearly averaging 8×8 analytical rays [9, p. 104] sampled across each detector cell. To focus on the projector accuracy, we used noiseless projection data.

We implemented iterative image reconstruction with these two projector/backprojector methods. We ran 50 iterations of the ordered subsets method with 82 subsets [10], initialized with reconstruction by the FDK method [11], for the following penalized weighted least-squares cost function with an edge-preserving ‘‘hyperbola’’ penalty function (PWLS-OS):

$$\Phi(\mathbf{x}) = \sum_i w_i \frac{1}{2} (y_i - [\mathbf{A}\mathbf{x}]_i)^2 + \beta R(\mathbf{x}) \quad (11)$$

$$R(\mathbf{x}) = \sum_k \psi([\mathbf{C}\mathbf{x}]_k), \quad (12)$$

where y_i is the negative log of the measured cone-beam projection, w_i values are statistical weighting factors, \mathbf{A} is the system matrix, \mathbf{C} is a finite differencing matrix and $\psi(t)$ is the potential function. Here we used the hyperbola:

$$\psi(t) = \frac{\delta^2}{3} \left(\sqrt{1 + 3(t/\delta)^2} - 1 \right). \quad (13)$$

For this simulation, we used $w_i = \exp(-[\mathbf{A}\mathbf{x}]_i)$, $\beta = 2$ and $\delta = 5$ Hounsfield units (HU).

For this iterative reconstruction experiment, we did not see obvious visual differences between reconstructions by the SF-TT and SF-TR method, and the normalized root-mean-square (NRMS) errors were similar. It appeared that the axial cone-beam artifacts due to poor sampling (not truncation) at the off-axis slices dominated other effects in the reconstructed images, such as the errors caused by rectangle approximation. Further research will evaluate these two projectors within iterative reconstruction methods under other CT geometries where the off-axis sampling is better, such as helical scans, yet where the cone angle is large enough to differentiate the SF-TT and SF-TR method.

IV. CONCLUSION

We have presented a 3D forward and back projector, named the SF-TT projector for X-ray CT. Our results have shown that the SF-TT projector is more accurate but computationally slower than the SF-TR projector. We demonstrated previously that the SF-TR projector is more accurate than the well-known DD projector but with similar computation speed in [1].

The SF-TT projector uses trapezoid functions in both the transaxial and axial directions. Using trapezoid functions in the axial direction involves more computation compared with using simple rectangular functions, such as projecting four axial boundaries of each voxel instead of two and evaluating the weight (contribution of a voxel to a detector cell) in two additional triangle areas of each trapezoid function. Thus it is reasonable that the computation time of the SF-TT projector was about 2 times that of the SF-TR projector. To save computation and maintain relative accuracy, one may use the original SF-TR projector for voxels that are near the X-ray source plane, where the cone angles are small and the rectangle approximation is reasonable, and use the SF-TT projector for other voxels.

ACKNOWLEDGMENT

We thank Dr. James Balter for ongoing discussions about cone-beam CT and GE for the use of their DD projector/backprojector code.

REFERENCES

- [1] Y. Long, J. A. Fessler, and J. M. Balter, ‘‘A 3D forward and back-projection method for X-ray CT using separable footprint,’’ in *Proc. Intl. Mtg. on Fully 3D Image Recon. in Rad. and Nuc. Med.*, 2009, pp. 146–9, winner of poster award.
- [2] —, ‘‘3D forward and back-projection for X-ray CT using separable footprints,’’ *IEEE Trans. Med. Imag.*, 2009, submitted as TMI-2009-0397.
- [3] R. L. Siddon, ‘‘Fast calculation of the exact radiological path for a three-dimensional CT array,’’ *Med. Phys.*, vol. 12, no. 2, pp. 252–5, Mar. 1985.
- [4] B. De Man and S. Basu, ‘‘Distance-driven projection and backprojection in three dimensions,’’ *Phys. Med. Biol.*, vol. 49, no. 11, pp. 2463–75, Jun. 2004.
- [5] A. Ziegler, T. Köhler, T. Nielsen, and R. Proksa, ‘‘Efficient projection and backprojection scheme for spherically symmetric basis functions in divergent beam geometry,’’ *Med. Phys.*, vol. 33, no. 12, pp. 4653–63, Dec. 2006.
- [6] S. Matej and R. M. Lewitt, ‘‘Practical considerations for 3-D image reconstruction using spherically symmetric volume elements,’’ *IEEE Trans. Med. Imag.*, vol. 15, no. 1, pp. 68–78, Feb. 1996.
- [7] C. Riddell and Y. Troussset, ‘‘Rectification for cone-beam projection and backprojection,’’ *IEEE Trans. Med. Imag.*, vol. 25, no. 7, pp. 950–62, Jul. 2006.
- [8] C. Schretter, ‘‘A fast tube of response ray-tracer,’’ *Med. Phys.*, vol. 33, no. 12, pp. 4744–8, Dec. 2006.
- [9] A. C. Kak and M. Slaney, *Principles of computerized tomographic imaging*. New York: IEEE Press, 1988.
- [10] H. Erdoğan and J. A. Fessler, ‘‘Ordered subsets algorithms for transmission tomography,’’ *Phys. Med. Biol.*, vol. 44, no. 11, pp. 2835–51, Nov. 1999.
- [11] L. A. Feldkamp, L. C. Davis, and J. W. Kress, ‘‘Practical cone beam algorithm,’’ *J. Opt. Soc. Am. A*, vol. 1, no. 6, pp. 612–9, Jun. 1984.